Supplement of Atmos. Meas. Tech., 15, 5545–5561, 2022
https://doi.org/10.5194/amt-15-5545-2022-supplement

Atmospheric Measurement Techniques
Open Access
EGU

Supplement of

A new hot-stage microscopy technique for measuring temperature-dependent viscosities of aerosol particles and its application to farnesene secondary organic aerosol

Kristian J. Kiland et al.

Correspondence to: Allan K. Bertram (bertram@chem.ubc.ca)

S1 Calibration of the hot-stage using substances with known melting points

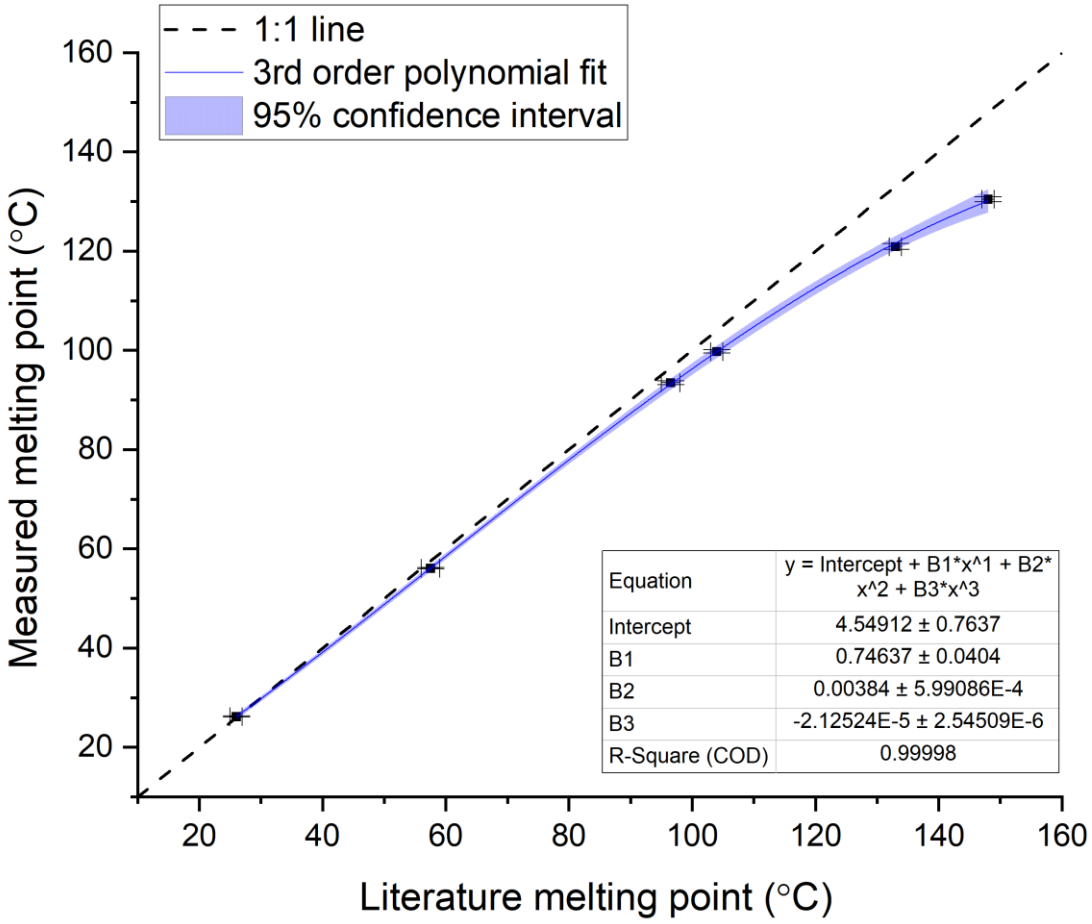

Figure S1 Calibration curve for the hot-stage microscopy apparatus. Each data point is the average of at least 4 melting point measurements for a substance with known melting point (In units of °C: diphenyl ether, 26 ± 1; 1-octadecanol, 57.5 ± 1.5; glutaric acid, 96.5 ± 1.5; pimelic acid, 104 ± 1; vanillyl mandelic acid, 133 ± 1; cholesterol, 148 ± 1). The *y*-error bars are the 95% standard error of the mean of the replicate measurements. The *x*-error bars are the uncertainties of the known melting points reported in the literature. The fit to the data is a 3rd order polynomial with 95% confidence bands. The dotted line shows a 1:1 relationship between the measured and literature melting point.

S2 Conditioning times of farnesene SOA

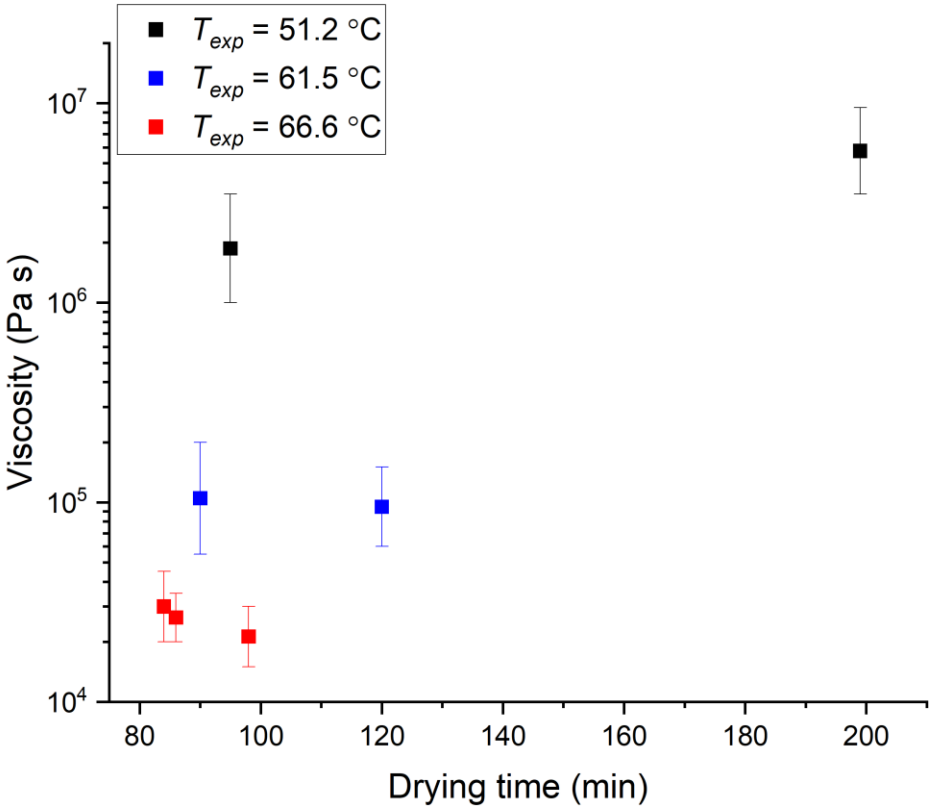

Figure S2 The viscosity of farnesene SOA material as a function of conditioning time. The viscosity was not strongly sensitive to conditioning times > 75 minutes.

S3 The effect of gravity during measurement

To illustrate that the effect of gravity on the shape of the particles is expected to be small, we compared the force of surface tension (F_{ST}) and the force of gravity (F_g) acting on a particle. The force of surface tension can be calculated with the following equation:

$$F_{ST} = 2\sigma\pi r \quad \text{(S1)}$$

Where σ is the surface tension and r is the radius of the droplet.

Assuming a spherical droplet, the force of gravity can be calculated with the following equation:

$$F_g = mg = \left(\frac{4}{3}\pi r^3 \rho\right) g \quad \text{(S2)}$$

Where r is the radius of the droplet, ρ is the density, and g = 9.8 $m^2\ s^{-1}$.

Assuming a particle diameter of 190 μm (the largest particle diameter from our experiments), a surface tension of 0.023 N m^{-1} (the smallest surface tension in our experiments), and a density of 1200 kg m^{-3}, F_{ST} is approximately a factor of 325 greater than F_g. The ratio of F_{ST} to F_g will be even larger for smaller droplets and larger surface tensions.

S4 Contact angle measurements

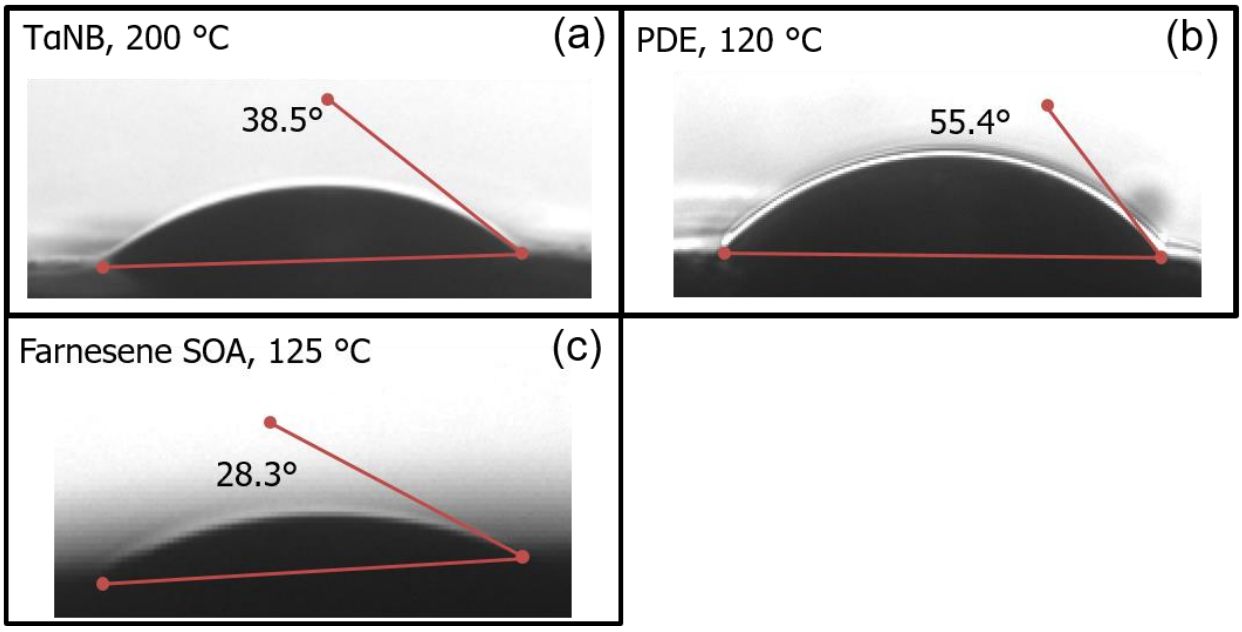

Figure S3 Examples of contact angle measurements for **(a)** TαNB, **(b)** PDE, and **(c)** farnesene SOA. The temperature was heated to the point where the substances had completely liquefied, reaching an equilibrium geometry. The angle tool in ImageJ was used to measure the contact angle.

S5 Summary of hot-stage microscopy viscosity measurements

Table S1 Results of TαNB hot-stage microscopy experiments. T_{exp} is the experimental temperature. The uncertainty in T_{exp} is a combination of temperature fluctuations and uncertainty in the temperature stage calibration. $\tau_{exp,flow}$ is the experimental flow time to reach maximum roundness (R_{max}). The upper and lower limit of viscosity, η, was determined using fluid dynamics simulations.

TαNB Expt#	T_{exp} (°C)	$\tau_{exp,flow}$ (s)	R_{max}	η (Pa s) upper limit	η (Pa s) lower limit
1	$98.5\ ^{+2.2}_{-1.6}$	252	0.315	1.0×10^6	9.5×10^5
2	98.5 ± 1.6	50	0.636	5.0×10^5	2.0×10^5
3	$98.5\ ^{+1.9}_{-1.6}$	512	0.477	2.0×10^6	2.0×10^6
4	$104.3\ ^{+1.7}_{-1.9}$	144	0.468	3.5×10^5	2.0×10^5
5	$104.3\ ^{+2.1}_{-1.8}$	55	0.417	3.5×10^5	2.0×10^5
6	104.3 ± 1.8	80	0.592	3.0×10^5	2.5×10^5

Table S2 Results of PDE hot-stage microscopy experiments. T_{exp} is the experimental temperature. The uncertainty in T_{exp} is a combination of temperature fluctuations and uncertainty in the temperature stage calibration. $\tau_{exp,flow}$ is the experimental flow time to reach maximum roundness (R_{max}). The upper and lower limit of viscosity, η, was determined using fluid dynamics simulations.

PDE Expt#	T_{exp} (°C)	$\tau_{exp,flow}$ (s)	R_{max}	η (Pa s) upper limit	η (Pa s) lower limit
1	$35.6\,^{+0.9}_{-0.6}$	2000	0.750	4.5×10^7	3.5×10^7
2	$35.6\,^{+1.0}_{-0.6}$	4500	0.701	2.5×10^6	1.5×10^6
3	$40.9\,^{+1.9}_{-0.6}$	765	0.753	5.0×10^5	2.5×10^5
4	$40.9\,^{+2.0}_{-0.6}$	198	0.784	2.0×10^5	1.5×10^5
5	$40.9\,^{+1.7}_{-0.6}$	36	0.734	1.5×10^5	1.5×10^5
6	$46.1\,^{+2.0}_{-1.3}$	32	0.621	9.5×10^4	7.5×10^4
7	$47.5\,^{+0.8}_{-0.8}$	7	0.640	2.5×10^4	5.0×10^3
8	$46.1\,^{+2.0}_{-0.6}$	40	0.717	3.5×10^4	3.0×10^4

Table S3 Results of hot-stage microscopy experiments with farnesene SOA material. T_{exp} is the experimental temperature. The uncertainty in T_{exp} is a combination of temperature fluctuations and uncertainty in the temperature stage calibration. $\tau_{exp,flow}$ is the experimental flow time to reach maximum roundness (R_{max}). The upper and lower limit of viscosity, η was determined using fluid dynamics simulations.

Farnesene SOA material Expt#	T_{exp} (°C)	$\tau_{exp,flow}$ (s)	R_{max}	η (Pa s) upper limit	η (Pa s) lower limit
1	$51.2\ ^{+1.1}_{-0.7}$	2500	0.354	3.5×10^6	1.0×10^6
2	$51.2\ ^{+1.3}_{-0.7}$	4900	0.588	9.5×10^6	3.5×10^6
3	$61.5\ ^{+1.7}_{-0.7}$	150	0.715	2.0×10^5	5.5×10^4
4	$61.5\ ^{+1.2}_{-0.7}$	150	0.809	1.5×10^5	6.0×10^4
5	$66.6\ ^{+2.0}_{-0.7}$	40	0.844	4.5×10^4	2.0×10^4
6	$66.6\ ^{+2.0}_{-0.7}$	35	0.859	3.5×10^4	2.0×10^4
7	$66.6\ ^{+1.9}_{-0.7}$	60	0.715	3.0×10^4	1.5×10^4

S6 Fluid dynamics simulations: comparing 2-D and 3-D

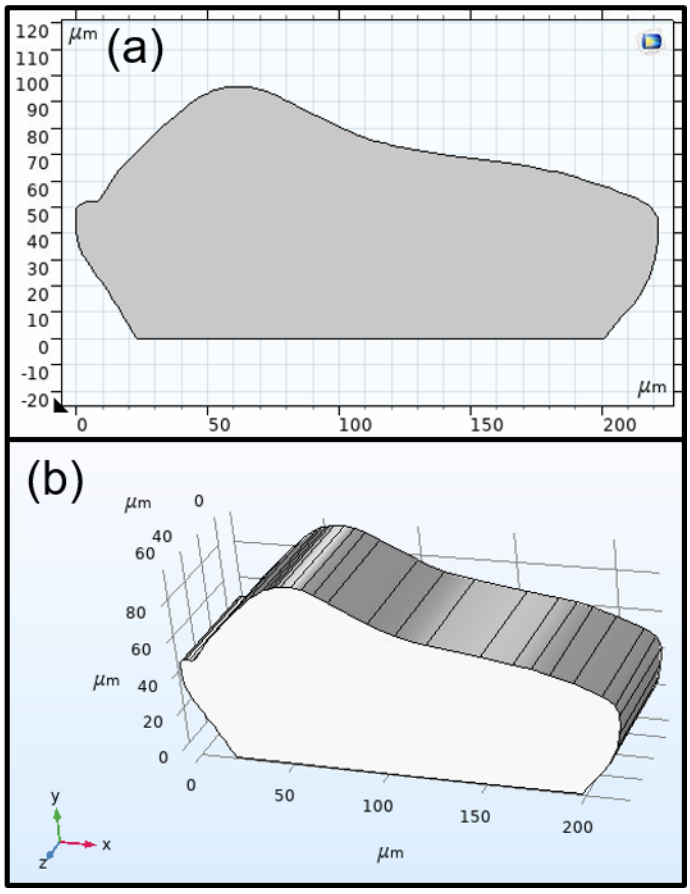

Figure S4 Example comparison of **(a)** 2-D and **(b)** 3-D geometries used for fluid dynamics simulations. The 2-D geometry was imported into COMSOL Multiphysics directly from the observed geometry. The 3-D geometry was made by extruding the 2-D geometry by an amount calculated based on conservation of mass and assuming the final geometry to be a spherical cap.

Table S4 Simulated viscosities for both 2-D and 3-D geometries. 2-D geometries were directly imported to COMSOL from the images captured on the hot stage microscope (after binarization). The 3-D geometries used the same shape as in 2-D, except they were extruded in the z-direction to give the particle depth. The depth was calculated using conservation of mass and assuming the final geometry was a spherical cap. Following the viscosity values, in the parenthesis, is the input combination of surface tension and slip length which gave the upper/lower limit. U_{ST}, U_{slip}, L_{ST}, and L_{slip} correspond to the upper limit of surface tension, the upper limit of slip length, the lower limit of surface tension, and the lower limit of slip length, respectively.

Experiment	Simulation	2-D geometry η (Pa s), (simulation inputs)	3-D geometry η (Pa s), (simulation inputs)	η ratio (2D/3D)
TαNB (T = 104.3 °C, Expt# 4)	Upper limit	3.5×10^5 (U_{ST}, L_{slip})	2.0×10^5 (U_{ST}, L_{slip})	1.75
	Lower limit	2.0×10^5 (U_{ST}, U_{slip})	2.0×10^5 (L_{ST}, L_{slip})	1.0
Farnesene SOA material (T = 51.2 °C, Expt# 2)	Upper limit	9.5×10^6 (U_{ST}, L_{slip})	9.5×10^6 (U_{ST}, U_{slip})	1.0
	Lower limit	3.5×10^6 (L_{ST}, U_{slip})	3.5×10^6 (L_{ST}, L_{slip})	1.0

S7 Chemical composition of farnesene SOA based on mass spectrometry

The combined mass spectra for farnesene photooxidation SOA in positive and negative mode are shown as a function of neutral mass and normalized to the largest peak in each mode (Figure S5). The top five neutral masses assigned in positive and negative mode are labelled in Figure S5.

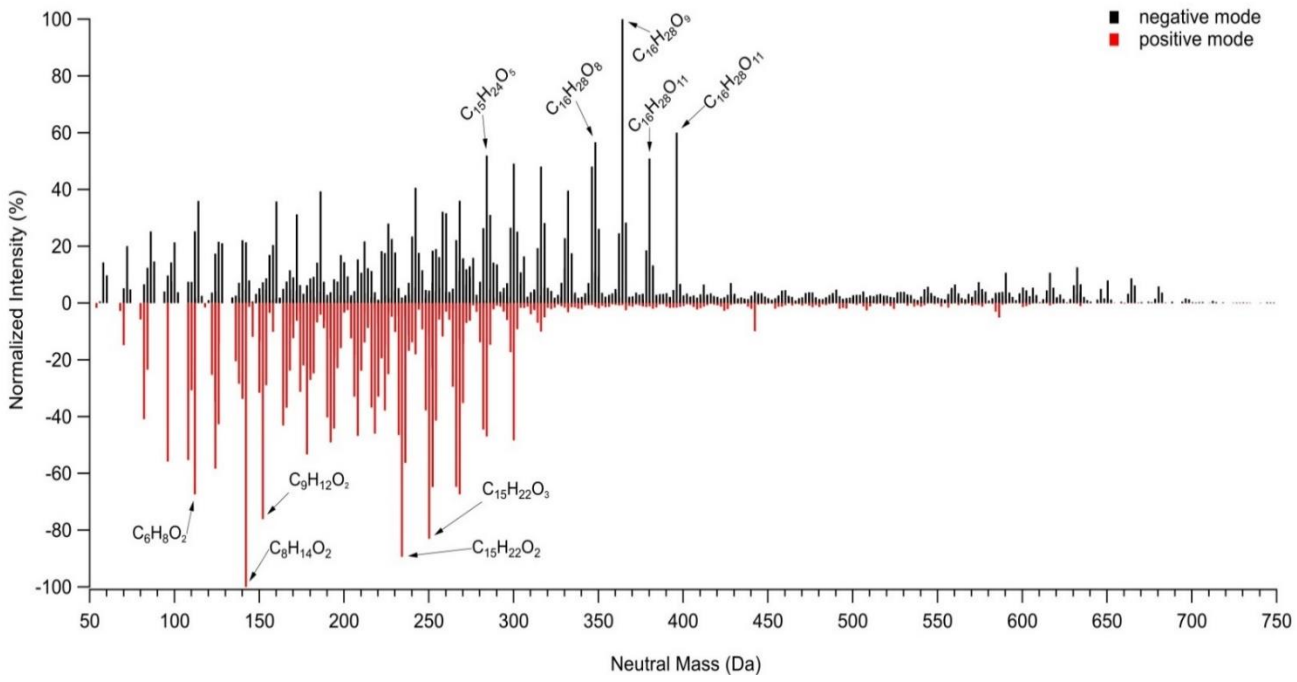

Figure S5 High resolution mass spectrometry of farnesene photooxidation SOA taken in the positive (red) and negative mode (black) ESI. The signals were normalized to the highest intensity in each respective mode. The five most abundant peaks in each mode are labeled by the corresponding neutral molecular formulas.

The mass spectra show larger abundance of higher molecular weight species in negative mode compared to positive mode with 1125 and 602 assigned compounds in each mode, respectively. The mass spectra for both modes show greater abundance of lower molecular weight compounds (< 250 Da) than generally observed with cyclic sesquiterpenes (Maclean et al., 2021), indicating the farnesene SOA compounds are fragmenting during the formation of SOA which is expected for an acyclic terpene. Few studies have investigated farnesene photooxidation SOA composition and properties (Jaoui et al., 2016; Kourtchev et al., 2012); however, some of the previously identified species are seen in the SOA from this study including C15 compounds such as conjugated triene alcohols ($C_{15}H_{24}O$ and $C_{15}H_{24}O_3$) and conjugated triene hydroperoxides ($C_{15}H_{24}O_2$ and $C_{15}H_{24}O_4$) and 2,3- epoxyfarnesol ($C_{15}H_{26}O_2$) which were also reported previously (Jaoui et al., 2016). Other SOA products tentatively identified include $C_8H_{16}O_3$

(5,6-dihydroxy-6-methyl-heptanone) and $C_{12}H_{18}O_2$ (4-methyl-8-methylene deca-4,9-dienoic acid) (Jaoui et al., 2016). Additional tentatively identified compounds in the mass spectra included several reported products previously identified from the gas phase and shown in Table S5. A portion of the compounds previously identified as gas-phase products were carbonyl compounds such as $C_3H_4O_2$ (methylglyoxal) and C_4H_8O (2-butanone). Alcohols can add to aldehyde or ketone functional groups of carbonyl compounds, forming hemiacetals and acetals whose formation would explain their presence in the condensed-phase mass spectra, consistent with previous work (Lim et al., 2010; Nguyen et al., 2011; Yasmeen et al., 2010; Ziemann and Atkinson, 2012).

Table S5 Compounds found in UPLC-PDA-ESI-HRMS for farnesene photooxidation SOA, consistent with previous literature with associated normalized intensity for each compound found in the overall positive and negative mode combined mass spectra. Class of compound is categorized based on what previous literature reported these products as.

Neutral Mass (Da)	Neutral Molecular Formula	Normalized Intensity (%)	Class of compound	References
268.167	$C_{15}H_{24}O_4$	100	Conjugated triene hydroperoxide (SOA product)	Jaoui et. al, 2016
112.052	$C_6H_8O_2$	90	SOA product	Kourtchev et al., 2012 Jaoui et al., 2016
252.173	$C_{15}H_{24}O_3$	80	conjugated triene alcohol (SOA product)	Jaoui et al., 2016
96.058	C_6H_8O	63	gas-phase product	Jaoui et al., 2016
236.178	$C_{15}H_{24}O_2$	55	conjugated triene hydroperoxide (SOA product)	Jaoui et al., 2016
110.073	$C_7H_{10}O$	35	gas-phase product	Kourtchev et al., 2012 Jaoui et al., 2016
84.058	C_5H_8O	35	gas-phase product	Jaoui et al., 2016
160.110	$C_8H_{16}O_3$	35	keto acid (SOA product)	Jaoui et al., 2016
100.052	$C_5H_8O_2$	21	gas-phase product	Kourtchev et al., 2012 Jaoui et al., 2016
72.021	$C_3H_4O_2$	19	gas-phase product	Jaoui et al., 2016
194.131	$C_{12}H_{18}O_2$	19	keto acid (SOA product)	Jaoui et al., 2016
126.104	$C_8H_{14}O$	14	gas-phase product	Kourtchev et al., 2012 Jaoui et al., 2016
58.042	C_3H_6O	14	gas-phase product	Jaoui et al., 2016
98.037	$C_5H_6O_2$	14	SOA product	Jaoui et al., 2016

114.068	$C_6H_{10}O_2$	14	gas-phase product	Jaoui et al., 2016
220.183	$C_{15}H_{24}O$	14	conjugated triene alcohol (SOA product)	Jaoui et al., 2016
60.021	$C_2H_4O_2$	9	gas-phase product	Jaoui et al., 2016
98.073	$C_6H_{10}O$	7	gas-phase product	Jaoui et al., 2016
74.037	$C_3H_6O_2$	5	gas-phase product	Jaoui et al., 2016
238.193	$C_{15}H_{26}O_2$	4	2,3- epoxyfarnesol	Jaoui et al., 2016
84.021	$C_4H_4O_2$	3	gas-phase product	Jaoui et al., 2016
72.058	C_4H_8O	2	gas-phase product	Jaoui et al., 2016
86.073	$C_5H_{10}O$	0.7	gas-phase product	Jaoui et al., 2016
180.151	$C_{12}H_{20}O$	0.1	gas-phase product	Jaoui et al., 2016

Shown in Figure S6 is the distribution of the number of carbon atoms per assigned compound. This figure illustrates that there was a large abundance of C16 compounds assigned, in addition to C15 compounds. Several tests were done to try and identify if these C16 compounds were artifacts of the mass spectrometry analysis (e.g., cluster ions) or impurities. These C16 compounds were not present in the farnesene standard we used based on a GC-MS analysis. They were also not present in the gas phase in our clean chamber before SOA generation, as verified by PTR-MS. Since the UPLC eluent had 0.1% formic acid, an additional test was done with the farnesene OH SOA with direct infusion-ESI, comparing SOA extracted in 1:1 ACN:H_2O with SOA in 1:1 ACN:H_2O and 0.1% formic acid (solvents A and B for LCMS). These C16 compounds were present with and without the formic acid added to our solvents. Additionally, the C16 peaks were not seen in the solvent blanks or blank extracted clean foil. This suggests that the C16 compounds are likely not a result of adduct formation during ionization, but are present in the SOA sample. Currently, it is unclear how these C16 compounds could be formed during photooxidation, therefore more tests are needed to determine a possible reaction mechanism.

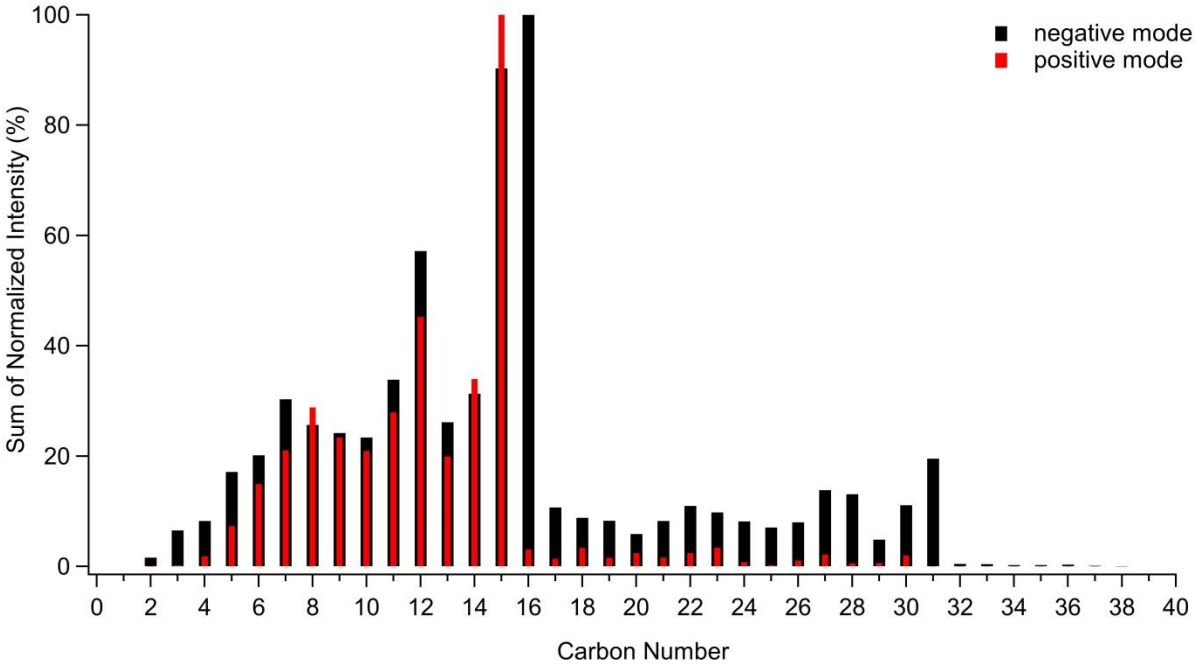

Figure S6 Sum of peak abundances of all molecular formula assignments based on carbon number for negative (black) and positive (red) mode ESI, normalized to the maximum intensity peak in each respective spectrum.

References:

Jaoui, M., Lewandowski, M., Docherty, K. S., Corse, E. W., Lonneman, W. A., Offenberg, J. H. and Kleindienst, T. E.: Photooxidation of farnesene mixtures in the presence of NOx: Analysis of reaction products and their implication to ambient PM2.5, Atmos. Environ., 130(x), 190–201, doi:10.1016/j.atmosenv.2015.10.091, 2016.

Kourtchev, I., Bejan, I., Sodeau, J. R. and Wenger, J. C.: Gas phase reaction of OH radicals with (E)-β-farnesene at 296 ± 2 K: Rate coefficient and carbonyl products, Atmos. Environ., 46, 338–345, doi:10.1016/j.atmosenv.2011.09.061, 2012.

Lim, Y. B., Tan, Y., Perri, M. J., Seitzinger, S. P. and Turpin, B. J.: Aqueous chemistry and its role in secondary organic aerosol (SOA) formation, Atmos. Chem. Phys., 10(21), 10521–10539, doi:10.5194/acp-10-10521-2010, 2010.

Maclean, A. M., Smith, N. R., Li, Y., Huang, Y., Hettiyadura, A. P. S., Crescenzo, G. V., Shiraiwa, M., Laskin, A., Nizkorodov, S. A. and Bertram, A. K.: Humidity-Dependent Viscosity of Secondary Organic Aerosol from Ozonolysis of β-Caryophyllene: Measurements, Predictions, and Implications, ACS Earth Sp. Chem., doi:10.1021/acsearthspacechem.0c00296, 2021.

Nguyen, T. B., Laskin, J., Laskin, A. and Nizkorodov, S. A.: Nitrogen-containing organic compounds and oligomers in secondary organic aerosol formed by photooxidation of isoprene, Environ. Sci. Technol., 45(16), 6908–6918, doi:10.1021/es201611n, 2011.

Yasmeen, F., Sauret, N., Gal, J. F., Maria, P. C., Massi, L., Maenhaut, W. and Claeys, M.: Characterization of oligomers from methylglyoxal under dark conditions: A pathway to produce secondary organic aerosol through cloud processing during nighttime, Atmos. Chem. Phys., 10(8), 3803–3812, doi:10.5194/acp-10-3803-2010, 2010.

Ziemann, P. J. and Atkinson, R.: Kinetics, products, and mechanisms of secondary organic aerosol formation, Chem. Soc. Rev., 41(19), 6582–6605, doi:10.1039/c2cs35122f, 2012.